Research in Astron. Astrophys. **2009** Vol. **9** No. **10**, 1103–1118
http://www.raa-journal.org *http://www.iop.org/journals/raa*

***R**esearch in*
***A**stronomy and*
***A**strophysics*

Statistical studies of optically dark gamma-ray bursts in the $Swift$ era

Wei-Kang Zheng[1,2], Jin-Song Deng[1] and Jing Wang[1]

[1] National Astronomical Observatories, Chinese Academy of Sciences, Beijing 100012, China; jsdeng@bao.ac.cn
[2] Graduate University of Chinese Academy of Science, Beijing 100049, China

Received 2009 April 29; accepted 2009 June 6

Abstract We compare the properties of optically dark GRBs, defined by the optical-to-X-ray spectral index $\beta_{\rm OX} < 0.5$, and normal ones discovered by the $Swift$ satellite before the year 2008 in a statistical way, using data collected from the literature and on-line databases. Our sample include 200 long bursts, 19 short bursts, and 10 with measured high redshifts ($z \gtrsim 4$). The ratio of dark bursts is found to be $\sim 10-20\%$, and is similar between long bursts, short ones, and the high-z sub-sample. The result for long bursts is consistent with both the pre-$Swift$ sample and studies by other authors on smaller $Swift$ samples. The existence of dark short GRBs is pointed out for the first time. The X-ray derived hydrogen column densities of dark GRBs clearly prefer large values compared with those of normal bursts. This supports the dust extinction scenario as the main cause of dark GRBs. Other possibilities like very high redshifts and non-standard emission mechanisms are less likely although not fully excluded.

Key words: gamma rays: bursts — gamma rays: observations

1 INTRODUCTION

There has been a long-standing problem of optically "dark" Gamma-Ray Bursts (GRBs) since the discovery of afterglows. Nearly 90% of well-localized GRBs have an identified X-ray afterglow (De Pasquale et al. 2003; Gehrels et al. 2007). However, some of them elude an optical detection. In the $BeppoSAX$ satellite era, over $\sim 60-70\%$ of GRBs with optical follow-ups failed to show an optical counterpart (Fynbo et al. 2001; Lazzati et al. 2002). The long time lag between BeppoSAX detection and the optical follow-up was suspected to be at least partly responsible since a GRB afterglow decays rapidly in brightness. The HETE-2 mission, with better GRB localizations and rapid coordinate dissemination ability, reduced the optical non-detection fraction to $\sim$ 10%, once claimed as the end of the "dark burst" mystery (Lamb et al. 2004).

The problem resurfaced quite unexpectedly in the $Swift$ era. The Burst Alert Telescope of the satellite can localize a triggered GRB with high precision ($\sim$ 3') almost instantly (Gehrels et al. 2004). The X-Ray Telescope and Ultra-Violet/Optical Telescope onboard routinely perform follow-up observations starting from just a few minutes after the onset of a GRB. A large global network of ground fast-response telescopes, on alert for a BAT GRB trigger, can slew for optical follow-ups within minutes (e.g., Zheng et al. 2008), followed then by big telescopes used for deep searches. Precise XRT localization ($\sim$ 5") helps in optical counterpart identifications. However, defying all those advantages, the detection rate in early UVOT observations ($<$ 1 hr) turned out to be only $\sim 30\%$ (Roming et al. 2006).

Recently, Melandri et al. (2008) and Cenko et al. (2009) found a significant incidence of dark bursts in their respective systematic ground follow-ups, which went deeper than the UVOT. Those authors utilized a more physical definition of dark bursts (Jakobsson et al. 2004), which evaluates the optical brightness relative to the X-rays.

Several suspects have been proposed as the cause of optical darkness. 1) For a GRB at very high redshift ($z \gtrsim 4$), the hydrogen Lyα blanketing and absorption of intervening host-galaxy or intergalactic medium may greatly suppress the flux in an observer-frame wavelength below $1215(1+z)$ Å (Lamb & Reichart 2000). However, GRBs with such a confirmed high redshift are still rare. 2) Extinction by dust in the host galaxy of a dark burst may be very high (e.g., Djorgovski et al. 2001; Rol et al. 2007; Jaunsen et al. 2008), working together with the relatively high GRB redshift which may shift UV photons, which have much larger extinction coefficients than optical ones, into the observing optical band (Klose et al. 2003). 3) The optical light curve may have decayed very rapid before the optical search started (e.g., Berger et al. 2002), a scenario seemingly no longer relevant in the $Swift$ era. 4) Last but not least, some GRBs may have an intrinsically low efficiency in optical afterglow emissions (e.g., Jakobsson et al. 2005; Oates et al. 2006; Urata et al. 2007) relative to X-rays, lower than that predicted by the standard afterglow model.

In this paper, we study the large sample of GRBs detected by the $Swift$ satellite up to the end of the year 2007, comparing the statistical properties between optically dark bursts and normal ones. Our sample and data selection are described in Section 2, and detailed analysis is in Section 3. Implications of our results for the various dark burst scenarios are discussed in Section 4. We compare our studies with similar ones in Section 5.

2 THE GRB SAMPLE AND DATA SELECTION

We selected a sample from the GRBs detected by $Swift$ BAT up to the end of the year 2007, collecting the redshift, BAT fluences between $15-150$ keV, R-band flux densities and X-ray integral fluxes of $0.2-10$ keV at 11 hr after the BAT trigger, and intrinsic hydrogen column density $N_{\rm H}$. The $0.2-10$ keV X-ray integral flux was converted to the flux density at 3 keV using the measured X-ray spectral index (or using the mean value 1.1 if no measured value was found). Optical fluxes have been corrected for Galactic extinction (Schlegel et al. 1998). We derived the optical-to-X-ray spectral index at 11 hr, $\beta_{\rm OX}$ ($F_\nu \propto \nu^{-\beta}$), from the ratio of the R-band flux density to the 3 keV one, in order to distinguish the optically dark bursts from the GRB sample (Jakobsson et al. 2004).

For the sake of convenience, we labeled our GRBs with optical detections as "OT" and those with only optical upper limits as "UL". We excluded GRBs without a detected X-ray afterglow since a measured X-ray flux is essential for our dark burst definition.

We chose Nysewander et al. (2009) as our main data source except for the $N_{\rm H}$ values. Those authors made a comprehensive data compilation of the GRBs with X-ray or optical follow-up observations detected before the year 2008 by various satellites and having, after a thorough literature search to find the best data. Note that if no 11-hr R-band or X-ray observational data were available, data extrapolation was done by them. For that purpose, a power-law temporal decay of the X-ray flux, with a slope of 1.2, that of the optical flux, with a slope of 0.85 for long bursts and of 0.68 for short bursts, and an optical spectral index of 1.0 were assumed. A similar compilation made by Gehrels et al. (2008) for the $Swift$ GRBs only extends to 2007 July. For some of the GRBs observed by Melandri et al. (2008), extrapolating the R-band upper limits reported there (usually of combined images) to 11 hr results in values significantly deeper than in Nysewander et al. (2009), so those deeper values were adopted. We replaced the R-band slope value 1.1, which was assumed in Melandri et al.(2008), with 0.85 when doing extrapolation in order to maintain data uniformity. Finally, we found three $Swift$ bursts, GRB 050502B, GRB 060602B, and GRB 060807, that were somehow missed from Nysewander et al. (2009). We included two of them, collecting data from other literature, but we rejected GRB 060602B which suffered from incredibly large Galactic extinction.

Two kinds of intrinsic $N_{\rm H}$ values were compiled by us. Both were derived from X-ray spectral data-reductions taking into account the host-galaxy gas absorption, with solar metallicity assumed, while the

Galactic $N_{\rm H}$ was fixed to the value of Dicky & Lockman (1990). For one kind, i.e., $N_{\rm H}^0$, the redshift of the host galaxy was simply fixed at zero. For the other, the measured host-galaxy redshift was adopted and we designated the fitting intrinsic column density as $N_{\rm H}^z$. We first collected the $N_{\rm H}^z$ values in Grupe et al. (2007), followed by more from the UK Swift/XRT GRB spectrum repository [1] (Evans et al. 2007), and the rest from other literature. For the GRBs without measured redshifts, the UK repository provided us with the $N_{\rm H}^0$ values, while for those of known z, we searched the GRB Coordinates Network [2] (GCN) Circulars and Reports for $N_{\rm H}^0$. The UK repository had not yet responded to a few cases of late reported z by the time this paper was written. For those, we multiplied $N_{\rm H}^0$ by $(1+z)^{2.1}$ to get empirical $N_{\rm H}^z$ values. The fitting $N_{\rm H}$ for the XRT Windowed Timing data and that for the Photon Counting data could be different if both were available; we chose the latter, as Butler & Kocevski (2007) suggested that it may better reflect the true value. In some cases, no gas absorption above the Galactic value was needed at all, so the intrinsic $N_{\rm H}$ value had to be left open.

Our final sample, which consists of 229 $Swift$ BAT GRBs in total, is listed in Tables 1 and 2. Among those, we seek out the ten with measured high redshifts ($z \gtrsim 4$) to make a high-z sub-sample (Table 2), whose R-band fluxes must have been significantly diluted by intergalactic H Lyman blanketing absorptions. The remaining 219 include 200 long bursts ($T_{90} > 2$ sec; Table 1) and 19 short bursts ($T_{90} < 2$ sec; Table 1). Note that all the high-z sub-sample members are also long bursts.

Following Jakobsson et al. (2004), we define dark bursts as those with $\beta_{\rm OX} < 0.5$. This definition has operational advantages over the "optical non-detection" one that was typically described by a more or less arbitrary threshold in the limiting apparent magnitude (e.g., $R \sim 23$ within 2 days; Djorgovski et al. 2001). More importantly, it has a clear physical meaning. The standard afterglow model assumes that there is synchrotron radiation from relativistic electrons accelerated by the forward-external shock. For slow cooling which is certainly the case at an epoch as late as 11 hr, the X-ray or optical spectrum above ν_c must be $\propto \nu^{-p/2}$, and that of $\nu_m < \nu < \nu_c$ proportional to $\propto \nu^{-(p-1)/2}$ (see Zhang & Mészáros 2004 for a review). Below ν_m, the spectrum can rise to higher frequencies but a corresponding rising light curve has not been observed at a late time, so this case can be excluded. The electron spectral index p is typically $\sim 2-2.5$. As for $p > 2$, which is most reasonable in shock acceleration physics, $\beta_{\rm OX}$ cannot be smaller than 0.5 in order to be compatible with the standard afterglow model. To allow for some measurement errors, we designated the boundary cases, i.e. with $0.5 < \beta_{\rm OX} < 0.6$, as "gray" bursts. Rol et al. (2005) proposed another method to identify dark bursts by comparing optical fluxes/upper limits with model extrapolations from the X-rays for any specific GRB. This may be more precise than using $\beta_{\rm OX}$, but it seems difficult to implement for a large sample.

3 DATA ANALYSIS

3.1 The optical flux versus X-ray flux diagram

The R-band flux densities and the 3-keV X-ray flux densities of our sample are plotted in Fig. 1. Both long bursts (*circles*) and short bursts (*triangles*) are included. For our high-z sub-sample ($z \gtrsim 4$), two kinds of $\beta_{\rm OX}$ values are shown (*squares* and *asterisks*; see §4.1). OT events are denoted by *filled* symbols, while UL events by *open* ones. Three lines are drawn to show the slope positions corresponding to $\beta_{\rm OX} = 0.5$ (*red*), 0.6 (*green*), and 1.25 (*black*), respectively. Most of our sample is confined between $\beta_{\rm OX} = 0.5$ and $\beta_{\rm OX} = 1.25$, as expected if $2 < p < 2.5$ in the context of the standard afterglow model.

Excluding the UL events, of which only the upper limits of $\beta_{\rm OX}$ are available, there is only one burst with $\beta_{\rm OX} > 1.25$. This is the peculiar GRB 060128, which is sub-luminous, an X-ray flash, and associated with a supernova (Pian et al. 2006), and its $\beta_{\rm OX} = 1.76$. Campana et al. (2006) claimed that its large first-day optical fluxes, behaving uniquely and peaking near 11 hr, were powered by SN shock breakout rather than a genuine GRB afterglow (see also Wang et al. 2007).

A significant fraction of both the OT events and UL events lies below the $\beta_{\rm OX} = 0.5$ criterion line, and hence are classified as dark bursts (*red* symbols). The true dark fraction could be underestimated

[1] http://www.swift.ac.uk/xrt_spectra/

[2] http://gcn.gsfc.nasa.gov/

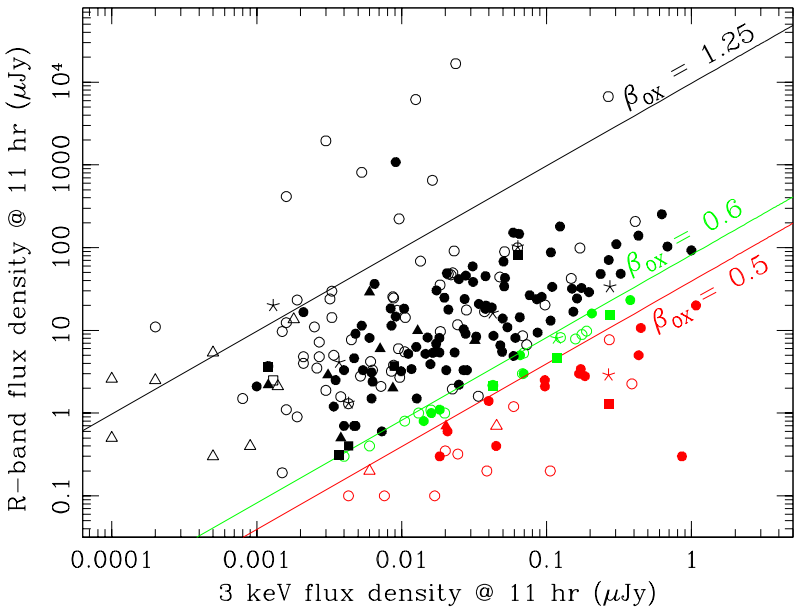

Fig. 1 R-band flux density versus the 3 keV X-ray flux density at 11 hr. Dark bursts ($\beta_{\rm OX} < 0.5$) are drawn in *red*, those of $0.5 < \beta_{\rm OX} < 0.6$ in *green*, and the others in *black*. *Triangles* present short bursts, and *circles* long bursts. A *filled* symbol means optical detection being reported (labeled OT), while an *open* one indicates optical upper limits only (labeled UL). For the 10 high-redshift bursts ($z \gtrsim 4$), two values are given for each (see §4.1), one *square* and the other *asterisk*. Also plotted are lines indicating $\beta_{\rm OX} = 0.5$ (*red*), 0.6 (*green*), and 1.25 (*black*), respectively.

since some UL events, with an upper-limit $\beta_{\rm OX}$ not much larger than 0.5, would have possibly turned out to be dark had their optical flux densities been measured. The majority of the dark bursts are long bursts and only three are short, while there are a few more long events, but no short ones, in the "gray" region ($0.5 < \beta_{\rm OX} < 0.6$; *green* symbols).

3.2 Short bursts

In terms of their $\beta_{\rm OX}$ distribution, the difference between the 19 short bursts and the long bursts is not significant, as indicated by the K-S test p-value which is 0.4 for OT events only or 0.2 if UL events are included. The optical afterglows of short bursts as a whole are fainter than those of long bursts (Kann et al. 2008), but so are their X-ray afterglows and prompt emissions (Nysewander et al. 2009). Consequently, they occupy the lower-left region of Fig. 1 (see also Gehrels et al. (2008) but for a much smaller sample). Compared with long bursts, they are not preferentially optically dark relative to X-rays.

In our sample, three short bursts are dark, i.e., one OT (GRB 070809) and two UL events (GRB 061210 and GRB 070724A). Gehrels et al. (2008), however, found no optically dark short bursts. We note that GRB 061210 (the XRT observation which started 2 d later) was not included in their sample, and neither was the optical upper limit of GRB 070724A. The classification of GRB 070809 is tricky since our $\beta_{\rm OX}$ value, 0.48, and theirs, 0.51, are actually very similar, both bordering the $\beta_{\rm OX} = 0.5$ separation line.

Although the $Swift$ satellite allows statistical studies on the optical darkness of short bursts to be performed for the first time, the current sample is still small. In the following sections, we will focus on the optical darkness of long bursts. GRB 060614 and GRB 060505 were also listed by us as long bursts despite the on-going hot debates on their exact nature (e.g., Fynbo et al. 2006; Zhang et al. 2007b).

3.3 Long bursts

The total dark ratio of our $Swift$ long burst sample is $\gtrsim 12\%$, or possibly even $\gtrsim 18\%$ if all the gray UL events are regarded as potential dark bursts. The ratio matches both the pre-$Swift$ result well, as concluded by Gehrels et al. (2008), and that of our short bursts. Including the 10 high-z events would not change the conclusion (see §4.1). By comparison, Cenko et al. (2009) reported a dark fraction as large as $\sim 50\%$ in the GRB sample that were followed up by the Palomar 60-inch telescope, and Melandri et al. (2008) found that most of the GRBs observed but undetected by the 2-m Liverpool and Faulkes telescopes are dark bursts. Those samples are much smaller than ours and their data inter-/extrapolation methods are somewhat different. The 23 Cenko GRBs before 2008 are all included in our sample, and contribute only 4 dark bursts and 2 gray ones according to our $\beta_{\rm OX}$ values. However, those authors only tabulated the $\beta_{\rm OX}$ values at 1000 sec. As a test, we interpolated or extrapolated their observed optical photometry to 11 hr and recalculated $\beta_{\rm OX}$ and obtained only 3 dark bursts and 3 gray ones. Regarding the $Swift$ GRBs in Melandri et al. (2008), as stated in Section 3.1, the R-band upper limit reported there was adopted in our sample if it resulted in the best available constraint on $\beta_{\rm OX}$.

The *left* panel of Fig. 2 shows the $\beta_{\rm OX}$ histograms of all the long bursts of our sample (*dashed black*) except for the high-z ones, *upper* for the 113 OT events and *lower* for the 87 UL ones. The distributions of the Jakobsson et al. (2004) sample of 52 pre-$Swift$ GRBs (*solid pink*) are also plotted for comparison.

The $Swift$ OT distribution is somewhat asymmetric, peaking around 0.8, with more below the peak value than above it. There are 13 dark bursts ($\beta_{\rm OX} < 0.5$) identified and 7 gray ones ($0.5 < \beta_{\rm OX} < 0.6$). The pre-$Swift$ sample is much smaller, which may account for its narrower distribution, among which Jakobsson et al. (2004) found no dark bursts. However, according to the statistics, the two samples are not significantly different, with a K-S test p-value as large as 0.9.

The $Swift$ UL distribution seems biased towards large $\beta_{\rm OX}$ compared with the OT events (K-S test p-value as small as 0.004), not unexpected since their $\beta_{\rm OX}$ values are simply also upper limits. However, one still finds 10 dark UL cases and 12 gray ones. Like the OT samples, the $Swift$ and pre-$Swift$ UL samples are also not significantly different, with a K-S test p-value of 0.2. Note that all the 5 dark bursts identified in the pre-$Swift$ sample were UL events.

As shown in the *upper right* panel of Fig. 2, the 11-hr 3-keV X-ray flux densities of the $Swift$ UL events are, on average, lower than the OT ones (K-S test p-value of 4×10^{-4}). The mean value of the former is $\sim 10^{-2.0\pm0.8}$ μJy, while the latter is $\sim 10^{-1.5\pm0.6}$ μJy. We have also found a similar trend regarding the BAT fluence of the two samples, although the statistical significance is not as high (K-S test p-value of 0.04). On the one hand, weaker gamma-ray bursts also tend to release less energy during the afterglow stage, both in X-rays and in optical photons. On the other hand, optical afterglow detections rely on quick and accurate BAT and XRT localizations to become efficient, the latter clearly being favored by large BAT fluence and large X-ray flux densities.

The optical afterglows of the $Swift$ OT events are on average much fainter than the pre-$Swift$ ones of Jakobsson et al. (2004), demonstrating not only the ever-improving ensemble of GRB-dedicated optical facilities but also the excellent synergy between $Swift$ detections and ground-based follow-up observations. The respective 11-hr R-band flux density distribution plotted in the *lower right* panel of Fig. 2 has a mean value of $\sim 0.03 \pm 0.1$ mJy for $Swift$ and of $\sim 0.2 \pm 0.8$ mJy for pre-$Swift$. The two distribution are different with a K-S test p-value as small as 0.008. The corresponding distributions of the UL events are however indistinguishable (K-S test p-value of 0.8).

4 DISCUSSIONS ON THE NATURE OF DARK BURSTS

4.1 The high-redshift scenario

We have singled out the 10 GRBs that have measured redshifts approximately higher than 4 (see Table 2), in order to check if some bursts are optically dark simply due to very high redshifts. For $z \gtrsim 4$, the observed R-band flux is greatly depressed by the strong intergalactic or interstellar H Lyman absorptions

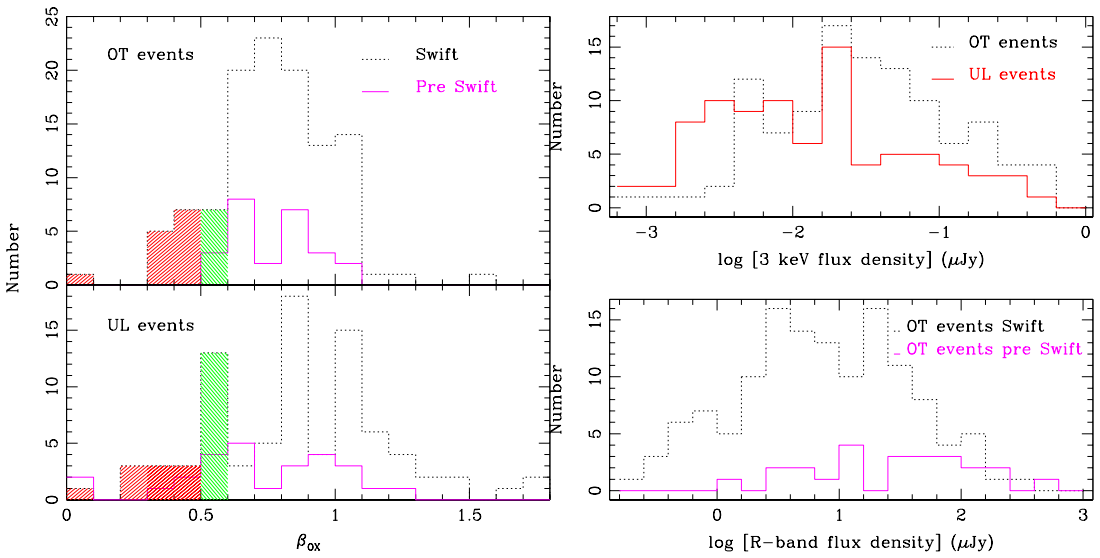

Fig. 2 *Left*: β_{OX} histogram distributions of the $Swift$ (*dashed black*) and pre-$Swift$ (*solid pink*) long bursts, with OT events shown in the *upper* panel and UL events in the *lower* panel. The filled color of *red* indicates dark bursts, while *green* shows gray bursts. *Upper right*: Histogram distributions of the X-ray afterglow flux density at 3 keV and 11 hr of the $Swift$ OT (*dashed black*) and UL (*solid red*) long bursts. *Lower right*: Histogram distribution of the R-band afterglow flux density at 11 hr of the $Swift$ OT long bursts (*dashed black*) compared with that of the pre-$Swift$ ones (*solid pink*; Jakobsson et al. 2004).

at $\lambda_{\rm obs} \leq 1025(1+z)$Å (Lamb & Reichart 2000). Two values of $\beta_{\rm OX}$ were calculated for each burst among the high-z sample. The first, $\beta_{\rm OX}1$, was obtained directly from the observed R-band flux, while to get $\beta_{\rm OX}2$ we extrapolated the observed NIR or IR flux (unaffected by Lyman absorptions for the given redshift) to the R band adopting a spectral index of 1.

It can be shown that the high-z H Lyman absorption does contribute to a few dark bursts, but it is unlikely to be a major factor for the $Swift$ GRB sample. Taking the $\beta_{\rm OX}1$ values, the high-z sub-sample members seem somewhat "darker" than those at lower redshifts. There are two events with $\beta_{\rm OX}1 \leq 0.5$ and three with $0.5 < \beta_{\rm OX}1 \leq 0.6$. On the other hand, the $\beta_{\rm OX}2$ values (i.e., having been de facto corrected for H Lyman absorptions) decrease the number of high-z dark bursts and those with gray ones both to 1. However, high-z GRBs identified so far are rare. Among the GRBs detected by $Swift$ and with measured redshifts, only a small fraction are located at $z \gtrsim 4$, or $\sim 10\%$ up to the end of the year 2007. However, we also sound a note of caution that, among our whole long GRB sample, 9 of the 13 dark OT events, 9 of the 11 dark UL pmes, and 10 of the 12 gray UL ones have no measured redshifts. Some would turn out to be high-z events if their redshifts were measured.

4.2 Dust extinction

It seems natural to hypothesize that dust extinction may account for at least some fraction of dark bursts, in view of the compelling evidence for the connection of long GRBs with the deaths of massive stars and with star-forming regions (see Woosley & Bloom 2006 and references therein). This scenario was first proposed by Groot et al. (1998) and Paczyński (1998) to explain the failed optical detection of GRB 970828, which can also be regarded as a prototypical dark burst by the $\beta_{\rm OX} < 0.5$ criterion of Jakobsson et al. (2004). However, as pointed out by Lazzati et al. (2002) and De Pasquale et al. (2003), it is complicated by theoretical predictions of possible dust destruction by strong GRB X-rays and/or UV flashes along the line of sight in the circumburst environment (e.g., Waxman & Draine 2000; Fruchter

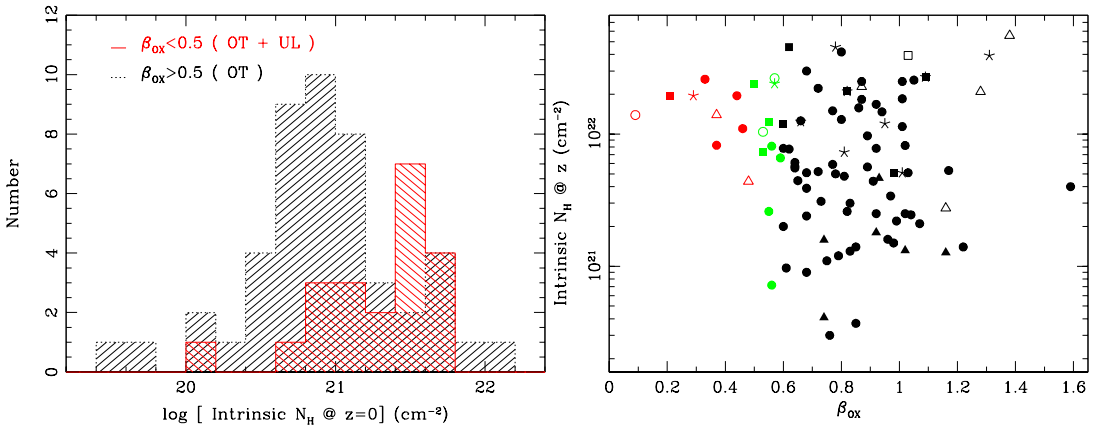

Fig. 3 *Left*: Histogram distribution of the intrinsic hydrogen column density $N_{\rm H}^0$ (assuming $z = 0$), in excess of the Galactic value, of dark bursts (*solid red*; both OT and UL events included) and normal ones (*dashed black*; OT only). *Right*: The same as in the left but for the value measured in the host galaxy's rest-frame $N_{\rm H}^z$. The meanings of the symbols and colors are the same as in Fig. 1.

et al. 2001). On the other hand, although still rare, highly extinguished GRBs were discovered in multi-band optical/IR observations, some of which are dark bursts according to $\beta_{\rm OX}$ (e.g., Rol et al. 2007; Tanvir et al. 2008; Jaunsen et al. 2008) while others seem not to be.

We used the hydrogen column density $N_{\rm H}$ as a proxy for the strength of local dust extinction to make statistical comparisons between dark bursts and normal ones, since the number of GRBs with known optical extinction values is far too low for such a purpose. The $N_{\rm H}(10^{22}\ {\rm cm}^{-2})/A_V$ value were estimated to be 0.18, 0.7, and 1.6 for the Milky Way, LMC, and SMC, respectively (see Schady et al. 2007 and references therein), although the values derived from GRB afterglow observations were, in general, much smaller possibly suggesting a lower dust-to-gas ratio in the GRB local environment (Galama & Wijers 2001; Stratta et al. 2004; Kann et al. 2006; Starling et al. 2007; but see Schady et al. 2007).

The $N_{\rm H}^0$ values for dark bursts are on average higher than for normal ones (*left* panel; Fig. 3). These are the X-ray absorption column densities in excess of the Galactic values, assuming zero redshift for the host galaxy (Evans et al. 2007). Neither short bursts nor high-redshift ones ($z \gtrsim 4$) are included. For dark bursts (*solid red*) both OT and UT events are included, while for normal ones (*dashed black*) only OT events are counted since some UL events of $\beta_{\rm OX} > 0.5$ could actually be dark. In total, 21 dark and 47 normal bursts are plotted in the figure. All but 5 of the dark bursts have $N_{\rm H}^0 > 10^{21}$ cm^{-2}, corresponding to a ratio of $\sim 76\%$, while the same high-$N_{\rm H}^0$ ratio for normal ones is only $\sim 40\%$. Applying a K-S test, we found that the probability that dark bursts and normal ones are drawn from the same $N_{\rm H}^0$ distribution is very small, only $\sim 0.4\%$. The histogram is only for long bursts. However, the conclusion is not changed by including short bursts, whose numbers are very small. Lin (2006) claimed somewhat different results, but his dark bursts just meant no-detection by the UVOT and in total only 25 $Swift$ GRBs were studied.

A more physically reasonable comparison can be made using the intrinsic $N_{\rm H}$ values in the rest frame of the GRB host galaxy, i.e., $N_{\rm H}^z$. Dark bursts are clearly inclined to have large $N_{\rm H}^z$ values despite possibly small statistics. This is shown in Fig. 3 by an $N_{\rm H}^z - \beta_{\rm OX}$ plot (*right* panel), instead of a histogram since the number of dark bursts whose $N_{\rm H}^z$ values are available is too small. Both long (*circles*) and short bursts (*triangles*) are included, as well as high-redshift ones (*squares* and *asterisks*). All the 9 dark bursts plotted here (*red*) have $N_{\rm H}^z > 4 \times 10^{21}$ cm^{-2}, as do most of the gray ones (*green*). In contrast, the $N_{\rm H}^z$ value of about half of the normal events (*black*) is well below 4×10^{21} cm^{-2}.

For further evidence of dust extinction dominating the formation of dark bursts as suggested by their very large $N_{\rm H}$, we looked to the literature for any measured optical extinction values of the dark

bursts in our sample. Our search, though by no means comprehensive, resulted in 4 bursts, which are GRB 050401 ($A_V \approx 0.6$; Watson et a. 2006), GRB 060923A ($A_V \approx 3$; Tanvir et al. 2008), GRB 070306 ($A_V \approx 4.9$; Jaunsen et al. 2008), and GRB 070802 ($A_V \approx 0.8-1.5$; Elíasdóttir et al. 2009; see also Krühler et al. 2008). Remarkably, all of them experienced strong dust extinction. Moreover, after correcting for their local optical extinction values, all had $\beta_{\rm OX} > 0.5$, i.e., they were no longer optically dark! Note the X-ray flux densities that we compiled have already been corrected for gas absorptions because of the nature of the X-ray data reduction procedures (Evans et al. 2007).

Systematic rapid and deep afterglow observations simultaneously taken in many optical and NIR bands are required to reliably constrain the local dust-extinction characteristics for dark and normal bursts. The A_V values cited above were derived assuming one of the Milky Way, LMC, and SMC extinction laws, while the true cases in the GRB environments or host galaxies can be very different (Li et al. 2008). Such an observational campaign is already being realized in the ongoing GROND project (e.g., Krühler et al. 2008), as well as being proposed for future GRB space missions like SVOM (Basa et al. 2008), JANUS (Roming et al. 2008), and EXIST (Grindlay et al. 2009).

4.3 Non-standard emission mechanisms

Our studies do not exclude the possibility that some dark bursts are attributable to the intrinsic mechanism by which the GRB afterglow emissions are produced. As shown in the ***left*** panel of Fig. 3, one long dark burst does have a very low $N_{\rm H}^0$ value. This is GRB 060510A with $N_{\rm H}^0 = 1.1 \times 10^{20}$ cm^{-2}, corresponding to marginal apparent dust extinction in the Milky Way, LMC, or SMC $N_{\rm H}/A_V$ relationships. The redshift of the GRB is unknown. Of course, the intrinsic column density $N_{\rm H}^z$ could be much higher if it took place at a relatively high redshift. What is not included in the figure is the short dark GRB 070809 with $N_{\rm H}^0 = 1.2 \times 10^{20}$ cm^{-2}. Being a short GRB, it was very likely lying at $z < 1$ and hence $N_{\rm H}^z$ is also not expected to be large. Urata et al. (2007) also argued that the optical darkness of GRB 051028, which was detected by the HETE-2 satellite, cannot be explained by local dust extinction since the X-ray fitting $N_{\rm H}$ is consistent with the Galactic value.

The dark burst criterion adopted by us is defined in the context of the standard afterglow model. It assumes that both the X-ray and optical afterglows are just different segments of the same synchrotron radiation spectrum of relativistic electrons that are accelerated in the forward shock when the GRB ejecta collide with circumambient material (e.g., Sari et al. 1998). This paradigm has been seriously challenged in the $Swift$ era by several observational facts (see Zhang 2007a and references therein), in particular, the occurrence of an early shallow-decay phase in many X-ray afterglow light curves (e.g., Liang et al. 2007), which was not often accompanied by similar behavior in the optical band, and the remarkable paucity of a highly-expected achromatic LC jet break (e.g., Liang et al. 2008). Many remedies have been proposed, including time-dependent microphysical parameters (e.g., Fan & Piran 2006), the contribution by long-lived reverse shocks (e.g., Genet et al. 2007), X-rays dominated by "late prompt emission" (Ghisellini et al. 2007), the importance of inverse-Compton scattering (Panaitescu 2008), scattering of X-rays by dust (Shao & Dai 2007), etc. The X-ray and optical afterglows may result from different emission mechanisms or regions, e.g., from relativistic forward and reverse shocks respectively. This forward-reverse-shock model was proposed early on by Dai (2004) and then numerically studied by Yu & Dai (2007) (see also Genet et al. 2007). It may be the emission from one of the two shocks that leads to optically dark GRBs. In addition, for the pre-$Swift$ dark GRB 001025A, Pedersen et al. (2006) invoked an extra thermal component to fit the X-ray spectrum which also solves its optical-darkness puzzle. Also, the afterglow emissions in the case of an electron energy spectral index $p < 2$, which can naturally lead to $\beta_{\rm OX} < 0.5$, were calculated by Dai & Cheng (2001), although it is difficult to make compatible with general acceleration mechanisms.

Finally, as shown in Fig. 4, dark and normal bursts follow a similar correlation with the X-ray flux density and γ-ray fluence (***lower***; see also Gehrels et al. 2008), while dark bursts lie considerably below normal ones in the optical-γ diagram (***upper***). On the one hand, this indicates that early X-ray abnormalities like flares and the shallow decay do not increase the apparent ratio of dark bursts. On the

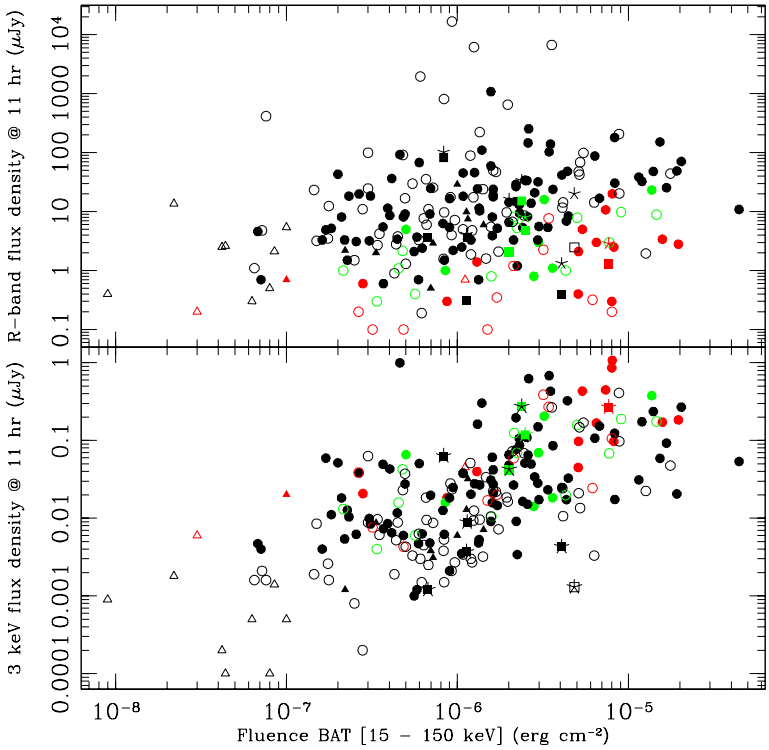

Fig. 4 R-band optical (*upper* panel) and 3 keV X-ray (*lower* panel) flux density at 11 hr as a function of the $Swift$ BAT fluence. The meanings of the symbols and colors are the same as in Fig. 1.

other hand, this may further support the dust-extinction hypothesis for dark bursts since they are clearly dim in the optical band rather than bright in X-rays.

5 COMPARISONS WITH OTHER STUDIES

We have compiled a large sample for statistical studies of the optical darkness of GRBs. The data set is uniform in the sense that all the GRBs were detected by the same instrument, i.e. the $Swift$ BAT. Gehrels et al. (2008) have calculated $\beta_{\rm OX}$ values or upper limits for a much smaller $Swift$ sample, consisting of only 41 long bursts and 10 short ones. On the one hand, they did not search for the GRBs detected in the last 5 months of 2007 which we have done. On the other hand, they only considered GRBs having optical measurements within a factor of 2 of 11 hr. Probably as a consequence, we have identified 3 dark short bursts but they found none. Notwithstanding, the dark ratio among long bursts is similar between the two studies and is also consistent with the pre-$Swift$ sample (De Pasquale et al. 2003; Jakobsson et al. 2004). In contrast, both Melandri et al.(2008) and Cenko et al.(2009) claimed a dark-burst occurrence as high as $\sim 50\%$ among the few dozen GRBs that have been observed with their specific optical telescopes. However, the light curve slopes adopted there for optical and X-ray data inter-/extrapolation are different from ours. Moreover, the $\beta_{\rm OX}$ in Cenko et al. (2009) was defined at 10^3 s. Nevertheless, their optical measurements have been taken into account when compiling our data set, but with necessary modifications to meet our data definitions.

There are other optical-darkness statistics performed on $Swift$ GRBs but using optical non-detection as the dark-burst definition, e.g., Lin (2006) and Balázs et al. (2008). The former found no systematic difference in X-ray $N_{\rm H}$ between their "dark" and "bright" groups, totaling 25 GRBs, while the latter came to a contradictory conclusion for a much larger sample. We cannot make direct compar-

isons between these results and ours. Nardini et al. (2008) compiled the R-band upper limits of optically non-detected $Swift$ GRBs to argue that most belong to their "underluminous optical" family. More recently, after the paper had been submitted, Perley et al. (2009) reported host galaxy studies of 14 "dark" GRBs, mixing optical non-detection and the $\beta_{\rm OX} < 0.5$ criterion in order to get a decent sample size. Like us, they identified dust extinction as the main cause of dark bursts. Finally, van der Horst et al. (2009) proposed a new definition for dark bursts, i.e., $\beta_{\rm OX} < \beta_{\rm X} - 0.5$ where $\beta_{\rm X}$ is the X-ray spectral index. By doing so, they can exclude the potential cases of $p < 2$ being classified as optically dark.

Acknowledgements We thank J. Hu, Y. Qiu, L. Xin, and J. Wei for stimulating discussions. This work was supported by the National Natural Science Foundation of China (Grant Nos. 10673014 and 10873017) and by the National Basic Research Program of China (Grant No. 2009CB824800). This research has made use of data supplied by the UK $Swift$ Science Data Center at the University of Leicester.

References

Balázs, L. G., et al. 2008, in AIP Conf. Proc., 1000, 44 (arXiv:0903.5275)
Basa, S., et al. 2008, in Proceedings of the Annual Meeting of the French Society of Astronomy and Astrophysics, eds. C. Charbonnel, F. Combes, & R.Samadi, 161 (arXiv:0811.1154)
Berger, E., et al. 2002, ApJ, 581, 981
Butler, N. R., Kocevski, D. 2007, ApJ, 668, 400
Cenko, S. B., et al. 2009, ApJ, 693, 1484
Campana, S., et al. 2006, Nature, 442, 1008
Curran, P. A., et al. 2007a, A&A, 467, 1049
Curran, P. A., et al. 2007b, MNRAS, 381, L65
Dai, Z. G., Cheng, K. S. 2001, ApJ, 558, L109
Dai, Z. G. 2004, ApJ, 606, 1000
De Pasquale, M., et al. 2003, ApJ, 592, 1018
Dickey, J. M., Lockman, F. J. 1990, ARA&A, 28, 215
Djorgovski, S. G., et al. 2001, ApJ, 562, 654
Duscha, S., et al. 2006, GCN Circ., 5417
Elíasdóttir, Á., et al. 2009, ApJ, 697, 1725
Evans, P., et al. 2007, A&A, 469, 379
Fan, Y. Z., Piran, T. 2006, MNRAS, 369, 197
Fruchter, A., Krolik, J. H., Rhoads, J. E. 2001, ApJ, 563, 597
Fynbo, J., et al. 2001, A&A, 373, 796
Fynbo, J., et al. 2006, Nature, 444, 1047
Galama, T. J., Wijers, R. 2001, ApJ, 549, L209
Gehrels, N., et al. 2004, ApJ, 611, 1005
Gehrels, N., Cannizzo, J. K., Norris, J. P. 2007, NJPh, 9, 37
Gehrels, N., et al. 2008, ApJ, 689, 1161
Genet, F., et al. 2007, MNRAS, 381, 732
Ghisellini, G., et al. 2007, ApJ, 658, L75
Goad, M., et al. 2005, GCN Circ., 3952;
Grindlay, J., et al. 2009, in AIP Conf. Proc., 1133, 18 (arXiv:0904.2210)
Groot, P. J., et al. 1998, ApJ, 493, L27
Grupe, D., et al. 2007, AJ, 133, 2216
Hurkett, C. P., et al. 2006, MNRAS, 368, 1101
Jakobsson, P., et al. 2004, ApJ, 617, L21
Jakobsson, P., et al. 2005, ApJ, 629, 45
Jakobsson, P., et al. 2006, A&A, 447, 897
Jaunsen, A. O., et al. 2008, ApJ, 681, 453

Kann, D. A., et al. 2006, ApJ, 641, 993
Kann, D. A., et al. 2008, ArXiv e-prints (arXiv:0804.1959)
Klose, S., et al. 2003, ApJ, 592, 1025
Krühler, T., et al. 2008, ApJ, 685, 376
Lamb, D. Q., Reichart, D. E. 2000, ApJ, 536, 1
Lamb, D. Q., et al. 2004, NewAR, 48, 423
Lazzati, D., et al. 2002, MNRAS, 330, 583
Li, A., et al. 2008, ApJ, 685, 1046
Liang, E. W., et al. 2007, ApJ, 670, 565
Liang, E. W., et al. 2008, ApJ, 675, 528
Lin, Y. Q. 2006, ChJAA (Chin. J. Astron. Astrophys.), 6, 555
Melandri, A., et al. 2006, GCN Circ., 5103;
Melandri, A., et al. 2008, ApJ, 686, 1209
Nardini, M., et al. 2008, ApJ, 386, L87
Nysewander, M., et al. 2009, ApJ, 701, 824
Oates, S. R., et al. 2006, MNRAS, 372, 327
Paczyński, B. 1998, ApJ, 494, L45
Panaitescu, A. 2008, ArXiv e-prints (arXiv:0811.1235)
Pandey, S. B., et al. 2006, A&A, 460, 415
Pedersen, K., et al. 2006, ApJ, 636, 381
Perley, D. A., et al. 2008, ApJ, 688, 470
Perley, D. A., et al. 2009, ArXiv e-prints (arXiv:0905:0001)
Pian, E., et al. 2006, Nature, 442, 1011
Prabhu, T. O. 2005, GCN Circ., 3346
Rol, E., et al. 2005, ApJ, 624, 868
Rol, E., et al. 2007, ApJ, 669, 1098
Roming, P. W., et al. 2006, ApJ, 652, 1416
Roming, P. W., et al. 2008, AAS, HEAD meeting, 10, 28.22
Ruiz-Velasco, A., E., et al. 2007, ApJ, 669, 1
Rumyantsev, V., et al. 2005, GCN Circ., 3939
Sakamoto, T., et al. 2008, ApJS, 175, 179
Sari, R., et al. 1998, ApJ, 497, L17
Schady, P., et al. 2007, MNRAS, 377, 273
Schlegel, D., et al. 1998, ApJ, 500, 525
Shao, L., Dai, Z. G. 2007, ApJ, 660, 1319
Starling, R., et al. 2007, ApJ, 661, 787
Stratta, G., et al. 2004, ApJ, 608, 846
Tanvir, N. R., et al. 2008, MNRAS, 388, 1743
Troja, E., et al. 2007, ApJ, 665, 599
Urata, Y., et al. 2007, PASJ, 59, L29
van der Horst, A. J., et al. 2009, ApJ, 699, 1087
Wang, X. Y., et al. 2007, ApJ, 664, 1026
Waxman, E., Draine, B. T. 2000, ApJ, 537, 796
Watson, D., et al. 2006, ApJ, 652, 1011
Woosley, S., Bloom J. 2006, ARA&A, 44, 507
Yu, Y. W., Dai, Z. G. 2007, A&A, 470, 119
Zhang, B. 2007a, ChJAA (Chin. J. Astron. Astrophys.), 7, 1
Zhang, B., Mészáros, P. 2004, IJMPA, 19, 2385
Zhang, B., et al. 2007b, ApJ, 655, 989
Zheng, W. K., et al. 2008, ChJAA (Chin. J. Astron. Astrophys.), 8, 693

Table 1. $Swift$ GRB sample catalog

ID	Redshift [†] z	BAT Fluence[‡] [15-150 keV] 10^{-7} erg cm^{-2}	Flux Density R @ 11h μJy	Flux Density 3 keV @ 11h 10^{-3} μJy	$\beta_{\rm OX}$ @ 11h	Intrinsic $N_{\rm H}$[⊕] @ $z=0$ 10^{21} cm^{-2}	Intrinsic $N_{\rm H}$[⊕] @ GRB z 10^{21} cm^{-2}
			Short	bursts			
OT							
$\beta_{\rm OX} < 0.5$							
070809		1.0	0.7	20.2	0.48	0.12	
$\beta_{\rm OX} \geq 0.6$							
050724	0.258	9.98	29.1	6.0	1.16		1.27[a]
051221A	0.547	11.50	7.5	32.0	0.74		1.58[a]
051227		6.99	0.5	3.8	0.66	0.79	
060313		11.30	9.9	12.9	0.90		
061006	0.4377	14.20	6.0	7.1	0.92		1.8[a]
061201	0.111	3.34	2.0	8.7	0.74	0.33	0.41[⊗]
070714B	0.92	7.2	2.9	3.1	0.93		4.65[a]
071227	0.383	2.2	2.2	1.2	1.02	0.57	1.32[⊗]
UL							
$\beta_{\rm OX} < 0.5$							
061210	0.4095	11.10	0.7	45.1	0.37	6.8	13.98[⊗]
070724A	0.457	0.3	0.2	6.0	0.48	1.99	4.39[⊗]
$\beta_{\rm OX} \geq 0.6$							
050509B	0.226	0.09	0.4	0.9	0.83		0.0018[a]
050813	1.8	0.44	2.6	0.1	1.38	6.4	55.62[⊗]
051210		0.85	2.1	1.4	1.00	2.5	
060801		0.80	0.5	0.1	1.16		2.75[a]
061217	0.827	0.42	2.5	0.2	1.28	5.9	20.92[⊗]
070209		0.22	13.6	1.8	1.22		
070429B	0.904	0.63	0.3	0.5	0.87	5.9	22.81[⊗]

Table 1 (continued)

ID	Redshift [†] z	BAT Fluence[‡] [15-150 keV] 10^{-7} erg cm^{-2}	Flux Density R @ 11h μJy	Flux Density 3 keV @ 11h 10^{-3} μJy	$\beta_{\rm OX}$ @ 11h	Intrinsic $N_{\rm H}$[⊕] @ $z = 0$ 10^{21} cm^{-2}	Intrinsic $N_{\rm H}$[⊕] @ GRB z 10^{21} cm^{-2}
070729		1.0	5.4	0.5	1.26	0.39	
			Long	bursts			
OT							
$\beta_{\rm OX} < 0.5$							
050219B		158.00	3.4	172.2	0.41	1.24	
050401	2.90	82.20	2.5	97.2	0.44		19.5[b]
050713A		51.10	2.1	97.3	0.42	2.61	
051008		50.90	0.4	44.9	0.30	3.15	
060510A		80.50	20.0	1072.1	0.40	0.11	
060923A		8.69	0.3	18.3	0.38	0.96	
061222A		79.90	0.3	858.2	-0.1	2.59	
070306	1.4959	53.80	5.0	431.7	0.33	3.34	26.0[e]
070419B		73.60	10.7	446.7	0.43	0.57	
070508	0.82	196.00	2.8	183.7	0.37	2.34	8.23[⊗]
070802	2.45	2.8	0.6	20.7	0.46		11.0[a]
071021		13	1.4	39.8	0.48	1.37	
071025		65	3.0	167.8	0.39	0.82	
$0.5 \leq \beta_{\rm OX} < 0.6$							
050315	1.949	32.20	16.0	205.2	0.59		6.6[b]
050915A		8.50	1.0	16.0	0.56	0.89	
060908	2.43	28.00	0.8	14.2	0.55		2.6[a]
061121	1.314	137.00	23.2	377.8	0.56		8.1[b]
070129		29.80	3.0	69.5	0.51	0.498	
070721B	3.626	36	1.1	18.3	0.56	0.029	0.72[⊗]
071118		5.0	5.0	65.6	0.59	1.55	
$\beta_{\rm OX} \geq 0.6$							
041223		167.00	25.4	92.4	0.76	0.31	
050126	1.29	8.38	1.5	6.2	0.75		1.1[a]
050215B		2.27	1.5	12.7	0.65		

Table 1 (continued)

ID	Redshift [†] z	BAT Fluence[‡] [15-150 keV] 10^{-7} erg cm^{-2}	Flux Density R @ 11h μJy	Flux Density 3 keV @ 11h 10^{-3} μJy	$\beta_{\rm OX}$ @ 11h	Intrinsic $N_{\rm H}$[⊕] @ $z = 0$ 10^{21} cm^{-2}	Intrinsic $N_{\rm H}$[⊕] @ GRB z 10^{21} cm^{-2}
050306		115.00	38.5	31.1	0.97		
050318	1.44	10.80	45.2	37.9	0.96		1.6[b]
050319	3.24	13.10	24.3	162.1	0.68		0.9[a]
050406	2.44	0.68	4.6	4.7	0.94	1.1	14.73[⊗]
050416A	0.6535	3.67	5.5	49.3	0.64		6.1[b]
050525A	0.606	153.00	151.9	58.9	1.07		2.1[b]
050603	2.821	63.60	87.6	107.0	0.91		4.4[a]
050607		5.92	0.7	4.7	0.68	0.6	
050712		10.80	18.2	37.8	0.84	0.4	
050721		36.20	23.8	85.7	0.77	1.25	
050801	1.56	3.10	18.4	8.4	1.05	5.1	25.60[⊗]
050802	1.71	20.00	14.4	65.3	0.73	0.263	3.1[b]
050820A	2.612	34.40	103.2	681.8	0.68	0.262	3.89[⊗]
050824	0.83	2.66	19.9	38.3	0.85		0.37[a]
050826	0.297	4.13	36.4	6.5	1.17		5.3[b]
050908	3.350	4.83	8.1	6.0	0.98	0.21[c]	
050915B		33.80	5.4	23.2	0.74	1.8	
050922C	2.198	16.20	23.9	27.2	0.92		2.5[a]
051006		13.40	11.4	5.3	1.04	5.46	
051016B	0.9364	1.70	4.9	59.2	0.60		7.8[b]
051109A	2.346	22.00	29.0	196.2	0.68		5.1[a]
051109B	0.080	2.56	3.1	6.2	0.85	0.98	1.4[b]
051111	1.55	40.80	41.6	24.8	1.01		18.5[b]
051117A		43.40	6.9	17.3	0.82	0.81	
060108	2.03	3.69	0.6	7.3	0.60		2[a]
060110		15.70	59.4	30.9	1.03	0.41	
060111A		12.00	3.3	20.3	0.69	1.32	
060111B		16.00	3.9	15.8	0.75	2.2	
060115	3.53	17.10	5.2	14.6	0.80		12.9[b]
060116[⊛]		24.10	5.34	16.4	0.79	5.74	
060124	2.296	4.61	92.8	997.2	0.62		7.7[b]
060202	0.783	21.30	3.3	26.7	0.66	3.74	12.60[⊗]
060203		8.98	5.4	18.2	0.77	0.71	
060204B		29.50	3.3	28.2	0.65	1.16	
060218	0.0331	15.70	1082.2	9.1	1.59		4.0[b]
060323		6.22	2.4	6.3	0.81	0.041	
060418	1.490	83.30	30.4	17.4	1.02		8.2[b]
060428A		13.90	110.0	302.8	0.80	1.33	
060428B		8.23	6.3	12.6	0.85	0.62	
060502A	1.51	23.10	9.4	86.7	0.64		5.7[b]
060505	0.089	9.44	2.2	24.8	0.61	0.81	0.97[⊗]

Table 1 (continued)

ID	Redshift [†] z	BAT Fluence[‡] [15-150 keV] 10^{-7} erg cm^{-2}	Flux Density R @ 11h μJy	Flux Density 3 keV @ 11h 10^{-3} μJy	$\beta_{\rm OX}$ @ 11h	Intrinsic $N_{\rm H}$[⊕] @ $z = 0$ 10^{21} cm^{-2}	Intrinsic $N_{\rm H}$[⊕] @ GRB z 10^{21} cm^{-2}
060507		44.50	8.4	32.7	0.76	0.48	
060512	0.4428	2.32	18.3	10.4	1.02		2.5[b]
060526	3.221	12.60	45.9	27.7	1.01		11.4[b]
060604	2.68	4.02	8.6	43.0	0.72		22.2[b]
060605	3.78	6.97	24.8	19.7	0.97		3.4[a]
060607A	3.082	25.50	33.6	109.3	0.78		5.0[b]
060614	0.125	204.00	70.8	268.5	0.76	0.143	0.3[b]
060707	3.425	16.00	8.1	60.9	0.67		
060708		4.94	9.1	27.6	0.79	0.31	
060714	2.711	28.30	20.9	34.1	0.87		18.3[b]
060729	0.54	26.10	253.3	623.7	0.82		2.6[b]
060804		5.98	67.9	50.4	0.98		
060904B	0.703	16.20	17.8	21.0	0.92		7.8[b]
060906	3.686	22.10	14.7	9.1	1.01		25.0[a]
060912A	0.937	13.50	10.3	26.8	0.81		4.8[b]
060926	3.208	2.19	3.3	5.4	0.87		25.0[a]
061007	1.261	444.00	10.9	53.6	0.72		5.2[b]
061019		25.90	146.4	64.7	1.05	6.9	
061021		29.60	31.9	149.8	0.73	0.443	
061110A	0.758	10.60	2.5	3.5	0.89		9.7[b]
061110B	3.44	13.30	0.7	4.8	0.68		30.0[a]
061126	1.1588	67.70	16.8	153.0	0.64	1.11	5.54[⊗]
061222B	3.355	22.40	1.2	3.4	0.80		41.8[b]
070110	2.352	16.20	18.9	41.9	0.83		1.3[d]
070208	1.165	4.45	3.4	11.7	0.77		5.9[a]
070224		3.05	3.2	9.9	0.79		
070318	0.836	24.80	34.0	51.0	0.89		5.64[a]
070330		1.83	5.2	11.1	0.84	0.68	
070411	2.954	27.00	13.9	49.7	0.77		15[a]
070419A	0.97	5.58	2.1	1.0	1.04		2.45[a]
070420		140.00	48.0	235.9	0.72	0.67	
070506	2.31	2.10	8.1	18.2	0.83		3.0[a]
070518		1.62	3.3	4.0	0.91	0.15	
070529	2.4996	25.70	8.2	15.1	0.86		15.8[a]
070611	2.04	3.91	11.4	8.5	0.98		1.5[a]
070616		192.00	49.0	20.5	1.06	0.85	
070628		35	139.4	430.0	0.79	0.92	
070721A		0.71	0.7	4.0	0.70	1.1	
070810A	2.17	6.9	9.1	4.8	1.03		5.1[a]
070911		120	32.5	174.0	0.71	0.73	
070917		20	6.6	47.9	0.67	14	

Table 1 (continued)

ID	Redshift [†] z	BAT Fluence[‡] [15-150 keV] 10^{-7} erg cm^{-2}	Flux Density R @ 11h μJy	Flux Density 3 keV @ 11h 10^{-3} μJy	$\beta_{\rm OX}$ @ 11h	Intrinsic $N_{\rm H}$ [⊕] @ $z = 0$ 10^{21} cm^{-2}	Intrinsic $N_{\rm H}$ [⊕] @ GRB z 10^{21} cm^{-2}
071003	1.60435	83	180.1	123.7	0.99	0.48	2.2[f]
071010A	0.98	2.0	43.0	51.6	0.92	4	16.79[⊗]
071010B	0.947	44	48.3	324.6	0.68		2.4[a]
071011		22	26.6	76.4	0.80	3.4	
071020	2.145	23	13.1	106.6	0.65	0.4	4.44[⊗]
071031	2.692	9.0	16.6	2.1	1.22		1.4[a]
071112C	0.823	30	5.6	17.3	0.79		1.2[a]
071122	1.14	5.8	3.7	1.2	1.09		1.8[a]
UL							
$\beta_{\rm OX} < 0.5$							
050713B[⊛]		31.80	2.26	387.6	0.24	2.15	
050716[⊛]		61.70	0.32	24.4	0.35	0.8	
060306		21.30	1.2	59.2	0.41	3.69	
060319[⊛]		2.64	0.20	38.7	0.23	4.06	
060719		15.00	0.1	16.9	0.24	3.91	
061202		34.20	7.7	270.9	0.46	5.12	
070219		3.19	0.1	7.6	0.35	3.19	
070223[⊛]		17.00	0.35	20.0	0.39	4.5	
070412		4.84	0.1	4.3	0.43	1.24	
070521	0.553	80.10	0.2	106.0	0.09	5.53	13.94[⊗]
$0.5 \leq \beta_{\rm OX} < 0.6$							
050128[⊛]		50.20	7.87	158.2	0.53	0.091	
050502B[*]		4.78	2.16	42.6	0.53	0.082	
050803	0.422	21.50	8.2	124.7	0.57	1.34	26.5[b]
050922B		22.30	5.3	69.5	0.59	0.91	
060814	0.84	146.00	8.9	175.5	0.53	2.89	10.40[⊗]
060904A		77.20	3.0	68.2	0.52	1.43	
060923C		15.80	0.8	10.5	0.59	0.79	
061004		5.66	0.4	6.0	0.57	0.12	
070103		3.38	0.3	4.0	0.59	2.71	
070328		90.60	9.8	188.6	0.54	2.02	
070517		2.15	1.0	13.1	0.59	0.39	
070621		43	1.0	19.8	0.53	4.4	

Table 1 (continued)

ID	Redshift [†] z	BAT Fluence[‡] [15-150 keV] 10^{-7} erg cm^{-2}	Flux Density R @ 11h μJy	Flux Density 3 keV @ 11h 10^{-3} μJy	$\beta_{\rm OX}$ @ 11h	Intrinsic $N_{\rm H}$[⊕] @ $z = 0$ 10^{21} cm^{-2}	Intrinsic $N_{\rm H}$[⊕] @ GRB z 10^{21} cm^{-2}
$\beta_{\rm OX} \geq 0.6$							
050117		88.10	207.1	409.0	0.85		
050124[⊛]		11.90	89.3	51.3	1.02		
050219A		41.10	11.7	24.3	0.84	0.48	
050223	0.5915	6.36	7.7	4.5	1.01		
050326		88.60	20.3	97.5	0.73	1.44	
050410		41.50	14.3	10.6	0.98	0.01	
050412[⊛]		6.18	0.19	1.5	0.66	0.17	
050421		1.45	23.3	1.9	1.28	4.6	
050422		6.07	1955.2	3.0	1.82	0.94	
050509A		3.41	2.7	9.7	0.77	2.3	
050528[⊛]		4.48	3.79	8.8	0.83		
050714B		5.95	3.3	6.3	0.85	3.27	
050717		63.10	14.3	3.3	1.14	1.6	
050726		19.40	9.7	18.5	0.85	0.095	
050819		3.50	4.2	6.1	0.89	0.18	
050822		24.60	8.6	68.3	0.66	0.65	
050827		21.00	6.7	72.9	0.62	2.23	
050916		9.29	16739.7	23.6	1.83	1.2	
051001		17.40	2.1	7.2	0.77	1.53	
051016A		8.37	9.7	1.5	1.19	3.42	
051021B		8.35	813.1	5.3	1.63	0.48	
051117B		1.77	12.4	1.6	1.22	2.4	
060105		176.00	44.1	47.6	0.93	1.85	
060109		6.55	35.4	18.4	1.03	2.28	
060123	1.099	3.0	99.7	63.0	1.00	0.99	
060211A		15.70	5.5	10.5	0.85	0.45	
060211B		4.38	2.8	5.2	0.86	0.55	
060219		4.28	0.9	1.9	0.84	3.51	
060312		19.70	652.4	16.3	1.44	1.02	
060322		52.20	68.6	13.5	1.16	1.9	
060403		13.50	223.0	9.6	1.37	2.5	
060413		35.60	6702.5	266.5	1.38	6.9	
060421		12.50	6173.4	12.5	1.78	2.3	
060427		4.99	1.3	4.3	0.78	0.92	
060501		12.20	4.8	2.7	1.02	14	
060515		14.10	24.0	3.2	1.21	2340	
060602A[⊛]	0.787	51.23	48.0	21.0	1.06		

Table 1 (continued)

ID	Redshift [†] z	BAT Fluence[‡] [15-150 keV] 10^{-7} erg cm^{-2}	Flux Density R @ 11h μJy	Flux Density 3 keV @ 11h 10^{-3} μJy	$\beta_{\rm OX}$ @ 11h	Intrinsic $N_{\rm H}$ [⊕] @ $z = 0$ 10^{21} cm^{-2}	Intrinsic $N_{\rm H}$ [⊕] @ GRB z 10^{21} cm^{-2}
060712		12.40	17.5	9.3	1.03	1.46	
060717		0.65	1.1	1.6	0.89	2.6	
060805A		0.72	4.8	2.1	1.05	0.65	
060807[⋆]		4.94	16.84	37.3	0.83	1.05	
060813		54.60	98.9	169.8	0.87	0.64	
060825		4.53	1.09	15.9	0.58	0.63	
060919		5.46	29.8	3.3	1.24	9.3	
060923B		4.80	91.2	23.0	1.13	3	
060929[⊛]		8.30	1.58	3.8	0.82	1.05	
061002		6.77	11.0	2.5	1.14	2	
061028		9.66	7.2	2.7	1.07	0.34	
061102		2.79	11.0	0.2	1.49	0.86	
070107		51.70	42.4	147.9	0.77	0.5	
070220[⊛]		14.71	1.60	33.8	0.83	1.53	
070227		16.20	49.7	22.5	1.05	1	
070429A		9.10	17.6	28.0	0.88	0.38	
070509		1.75	3.5	2.6	0.98	4.2	
070520A		2.50	1.5	0.8	1.03	2.35	
070520B		9.25	4.0	2.1	1.03	1.28	
070531[⊛]		10.80	5.0	3.4	0.99	0.22	
070612B		16.80	47.0	21.9	1.04	4.7	
070704		126.5	1.952	22.4	1.18	4	
070714A		1.5	3.2	8.5	0.81	4.7	
070805		7.2	25.5	8.7	1.09		
070808[⊛]		12	1.88	3.0	0.88	8.3	
070920B		6.6	6.0	9.5	0.88		
071028A		3.0	24.6	8.8	1.08	0.18	
071101		0.76	415.3	1.6	1.70	2.6	

[§] R-band and X-ray fluxes mainly adopted from Nysewander et al. (2008) unless specified otherwise.

[†] http://www.mpe.mpg.de/~jcg/grbgen.html; http://swift.gsfc.nasa.gov/docs/swift/archive/grb_table.html/.

[‡] http://swift.gsfc.nasa.gov/docs/swift/archive/grb_table.html/; Sakamoto et al. 2008

[⋆] 050502B; supplemented by us: http://www.swift.ac.uk/xrt_curves/00116116/; Prabhu (2005).

[⋆] 060807; supplemented by us: http://www.swift.ac.uk/xrt_curves/00223217/; Duscha et al. (2006).

[⊛] Deeper optical observations of Melandri et al. (2008) were adopted to replace the Nysewander et al. (2008) values.

[⊕] References for $N_{\rm H}$: [a] http://www.swift.ac.uk/xrt_spectra/ (all $N_{\rm H}$ @ $z = 0$ values unless specified otherwise); [b] Grupe et al. 2007; [c] Goad et al. 2005; [d] Troja et al. 2007; [e] Jaunsen et al. 2008; [f] Perley et al. 2008.

[⊗] Values derived from $N_{\rm H}$ @ $z = 0$ multiplied by $(1 + z)^{2.1}$.

Table 2. $Swift$ high-redshift GRB catalog

ID	Redshift z	Fluence[‡] [15-150 keV] 10^{-7} erg cm^{-2}	Flux Density 3keV @ 11h $10^{-3}\mu$Jy	Flux Density[†] R @ 11h μJy	$\beta_{\rm OX}1$ @ 11h	Flux Density[††] $R_{\rm ext}$ @ 11h μJy	$\beta_{\rm OX}2$ @ 11h	Intrinsic $N_{\rm H}$[⊕] @ GRB z 10^{21} cm^{-2}	[§] Ref
050505	4.27	24.90	117.7	4.7	0.50	8.0	0.57	24.0^b	1,2
050730	3.967	23.80	273.6	15.2	0.55	33.7	0.66	12.4^b	1,3
050814	5.3	20.10	42.4	2.1	0.53	16.2	0.81	7.3^a	1,4
050904	6.295	48.30	1.3	$<$2.48	$<$1.03	20.0	1.31	39.3^b	1,5
060206	4.048	8.31	63.2	82.7	0.98	101.9	1.01	5.1^a	1,6
060210	3.91	76.60	267.9	1.3	0.21	2.88	0.29	19.5^b	1,7
060223A	4.41	6.73	1.2	3.6	1.09		$>$1.09	27.0^a	1
060510B	4.9	40.70	4.3	0.4	0.62	1.32	0.78	45.5^b	1,8
060522	5.11	11.40	8.9	3.7	0.82		$>$0.82	21.0^a	1
060927	5.47	11.30	3.7	0.315	0.60	4.1	0.95	12.0^a	1,9

[‡]http://swift.gsfc.nasa.gov/docs/swift/archive/grb_table.html/; Sakamoto et al. 2008.

[†]True R-band observational results.

[††]Values extrapolated from the NIR/IR observations.

[⊕]References for $N_{\rm H}$ are the same as in Table 1.

[§]References: [1] Nysewander M. et al. 2008; [2] Hurkett et al. 2006; [3] Pandey et al. 2006; [4] Jakobsson et al. 2006; [5] Rumyantsev et al. 2005; [6] Curran et al. 2007b; [7] Curran et al. 2007a; [8] Melandri et al. 2006; [9] Ruiz-Velasco et al. 2007.